Calibration-Free Electrical Conductivity Measurements for Highly Conductive Slags

CHRISTOPHER J. MACDONALD, HUANG GAO, UDAY B. PAL,
JAMES VAN DEN AVYLE, and DAVID MELGAARD

This research involves the measurement of the electrical conductivity (κ) for the ESR (electroslag remelting) slag (60 wt.% CaF_2 – 20 wt.% CaO – 20 wt.% Al_2O_3) used in the decontamination of radioactive stainless steel. The electrical conductivity is measured with an improved high-accuracy-height-differential technique that requires no calibration. This method consists of making continuous AC impedance measurements over several successive depth increments of the coaxial cylindrical electrodes in the ESR slag. The electrical conductivity is then calculated from the slope of the plot of inverse impedance versus the depth of the electrodes in the slag. The improvements on the existing technique include an increased electrochemical cell geometry and the capability of measuring high precision depth increments and the associated impedances. These improvements allow this technique to be used for measuring the electrical conductivity of highly conductive slags such as the ESR slag. The volatilization rate and the volatile species of the ESR slag measured through thermogravimetric (TG) and mass spectroscopy analysis, respectively, reveal that the ESR slag composition essentially remains the same throughout the electrical conductivity experiments.

Sandia National Laboratories is a multiprogram laboratory operated by Sandia Corporation, a Lockheed Martin Company, for the United States Department of Energy under Contract DE-AC04-94AL85000

DISCLAIMER

DISCLAIMER

Portions of this document may be illegible in electronic image products. Images are produced from the best available original document.

I. INTRODUCTION

The stockpile of the Radioactive Scrap Metal (RSM) is continuously growing due to the downsizing and the decommissioning of nuclear facilities. Annually, the Department of Energy complexes produce approximately 120,000 metric tons of RSM. Contaminated stainless steel with high chromium and nickel contents accounts for 25-30% in weight of the generated RSM.[1] Disposal of this material not only represents significant resources and value lost, but also necessitates long term monitoring for environmental compliance. The latter results in an additional recurring expense. It is desirable to be able to decontaminate the radioactive stainless steel to a very low level that can be recycled or at least used for fabrication of containers for RSM disposal instead of using virgin stainless steel.

The goal of the RSM decontamination process is to reduce the radioactive contaminant to a sufficiently low level so that the metal can be handled safely or reused. Melt decontamination provides an effective means for consolidating and removing the contaminants from the bulk in a kinetically favorable manner. Various methods of melt decontamination evaluated are Electric Arc Melting, Air and Vacuum Induction Melting, Plasma Melting, and Electroslag Remelting (ESR). The ESR process has some inherent advantages in terms of cost, safety, and product quality.[2]

In the ESR process (Figure 1), the RSM forms one of the two electrodes. Joule heating through a molten slag layer maintains the slag temperature between 1700-2000°C and melts one end of the RSM electrode. The molten metal droplets from the consumable (RSM) electrode fall through the slag layer. While the metal is in contact with the slag, most of the radioactive contaminants from the metal are preferentially incorporated into the slag. The metal droplets are solidified in a water-cooled copper mold and form part of the consolidated and decontaminated

ingot underneath the slag layer. This can be easily formed into a useful product by mechanical processes such as rolling, forging, etc. The ingot also serves as the other electrode in the process. The slag containing the contaminants is removed as a solid and can be reused or appropriately disposed.

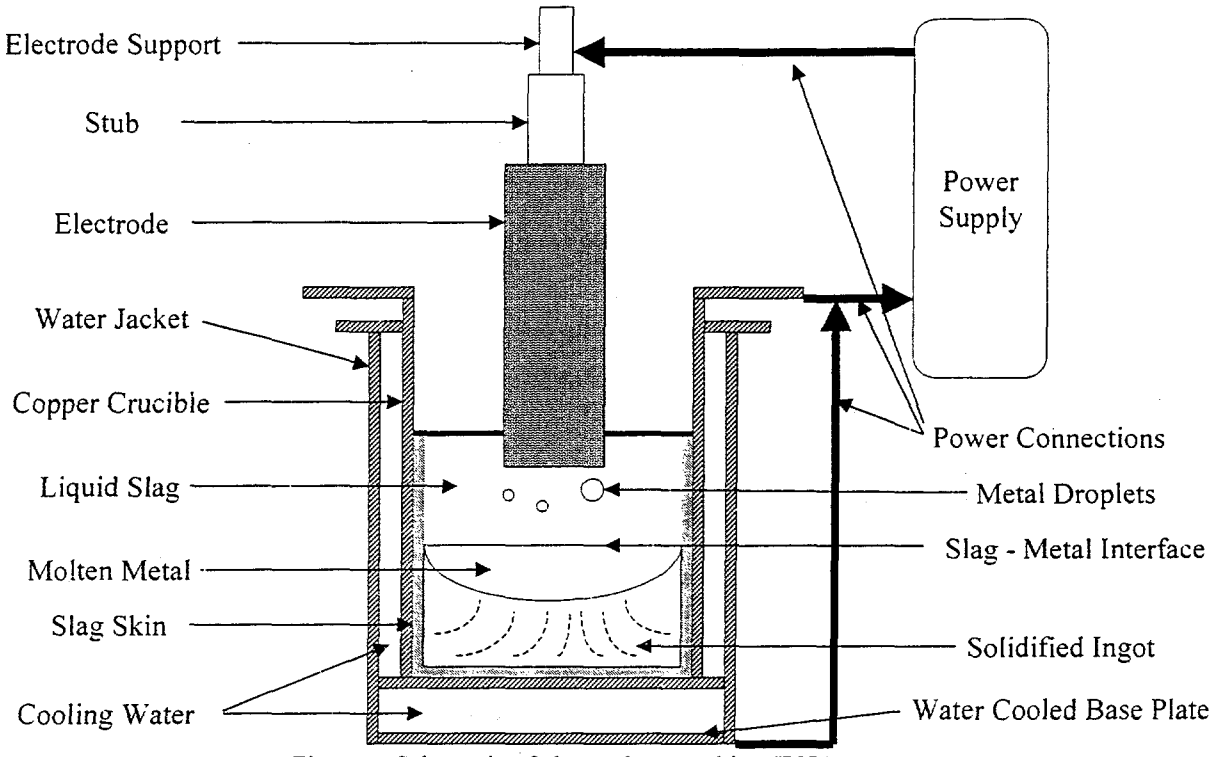

Figure 1: Schematic of electroslag remelting (ESR) process

In this study, the electrical conductivity of the ESR slag consisting of 60 wt.% CaF_2, 20 wt.% CaO, and 20 wt.% Al_2O_3 was measured as a function of temperature using the high-accuracy-height-differential technique. Henceforth, the ESR slag will also be referred to as the base slag. These measurements made with the high-accuracy-height-differential technique were compared to the baseline values obtained with the less accurate two point electrode method. The electrical conductivity of the base slag must be such that it provides efficient Joule heating in order to permit a reasonable melt rate. The liquid base slag serves as a resistive medium where the electrical energy from the applied current is converted into thermal energy. For a given

applied electrical potential between the electrodes, the current through the slag phase is dependent upon the electrical conductivity of the slag. Therefore, a more conductive base slag will produce a higher melt rate of the RSM due to the higher temperature in the slag phase. In the ESR process, the relationship of the power (P) used by the slag is shown in Equation 1,

$$P = VI = \frac{V^2 A \kappa}{d} \qquad [1]$$

where V is the applied electrical potential between the electrodes, I is the resulting current through the slag phase, d is the current path length, A is the cross sectional of the slag bath, and κ is the electrical conductivity of the slag.[3] A high melt rate of the RSM would result in a high production rate, however this condition would not necessarily optimize the end product (recycled stainless steel) in the ESR process. This is based on the modeling results reported by Choudhary and Szekeley.[4] They have shown that there are significant temperature gradients in the axial direction from the electrode-slag interface to the slag-metal interface in the ESR system. When the temperature at the top of the slag phase is considerably higher than the temperature at bottom of the slag phase (near the metal), then more molten metal solidifies at the water-cooled walls rather than the solidified ingot. Thus, the result is solidification of the decontaminated molten metal in the radial direction rather than the preferred axial direction. These temperature gradients in the axial direction also cause variations in the electrical conductivity and the Joule heating that is present throughout the slag phase. Conversely, a very low melt rate in the ESR process was shown to cause the solidified ingot to have coarse crystalline grains and poor surface finish. Hence, an accurate knowledge of the ESR slag conductivity is essential for optimizing the ESR process.

Secondly, the volatilization rate and the volatile species in the ESR process must be known in order to determine compositional variations of the slag and the associated electrical conductivity changes during the ESR process, and to establish an effective means of capture for the volatile species, if necessary. Therefore, the volatilization rate was also determined as a function of temperature of the base slag. The volatile species from the base slag were condensed and chemically analyzed. The volatilization rate and the volatile species were determined using a thermogravimetric (TG) balance and a quadropole mass analyzer, respectively.

II. THEORY

The high-accuracy-height-differential conductivity measurement technique requires no calibration.[5] Continuous AC impedance measurements are taken over a wide frequency range for each successive depth increment of a coaxial cylindrical electrode system in the slag. The simplified equivalent circuit of the system is shown in Figure 2,

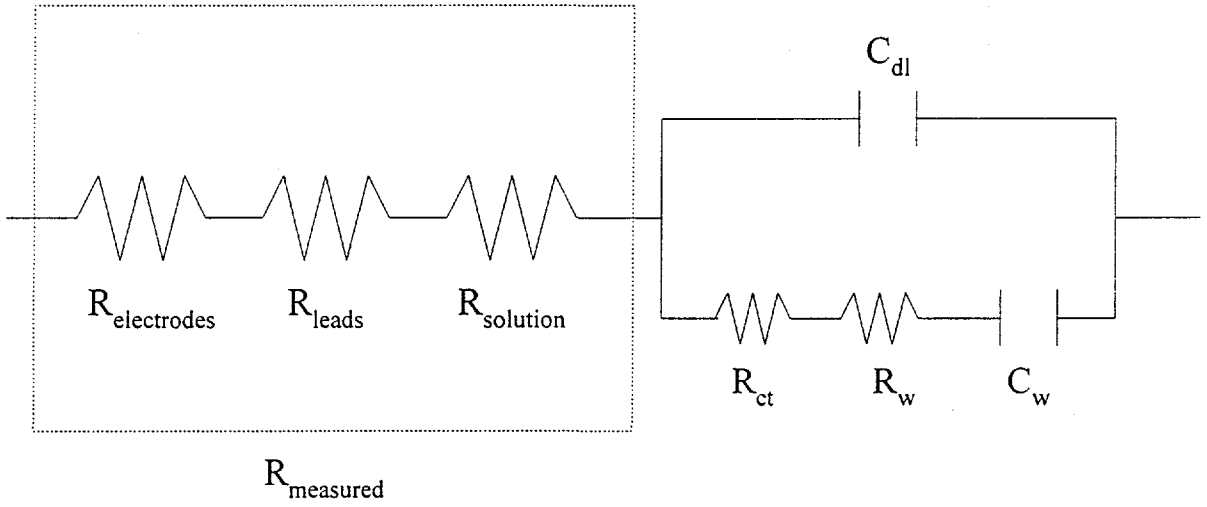

Figure 2: Equivalent circuit for the electrical conductivity measurement

where $R_{measured}$ is the measured resistance (impedance), $R_{electrodes}$ is the resistance of the electrodes, R_{leads} is the resistance of the leadwires, $R_{solution}$ is the resistance of the solution, C_{dl} is the double layer capacitance, R_{ct} is the resistance due to charge transfer, R_w is the Warburg[6]

resistance due to mass transfer, and C_w is the Warburg[6] capacitance due to mass transfer. At high frequencies, the double layer acts as a short circuit. Thus, the measured resistance ($R_{measured}$) or impedance ($Z_{measured}$) is the sum of the series of resistances (impedances) in Equation 2 with no contributions from the charge or mass transfer.

$$Z_{measured} = Z_{electrodes} + Z_{leads} + Z_{sol'n} \qquad [2]$$

The real component of the measured impedance ($Z_{measured}$) for a particular depth increment is determined by finding the x-intercept (when the value on the y-axis is equal to zero) via linear interpolation on the plot of real (Z_{real}) versus imaginary ($Z_{imag.}$) impedance, where the real and the imaginary impedance is plotted on the x-axis and y-axis, respectively. In order to determine the actual conductivity of the solution (base slag), the impedance of the electrodes ($Z_{electrodes}$) and leadwires (Z_{leads}) must be distinguished from the impedance of the solution ($Z_{sol'n}$). The values of impedance for the electrodes and leadwires are measured by shorting the electrodes of the system. Once the impedance of the solution is acquired for each depth increment, the inverse impedance of the solution ($1/Z_{sol'n}$) is plotted versus the corresponding depth. The slope of the straight line in this plot is used for calculating the electrical conductivity of the base slag.

The resistance (impedance) of the solution is related generically to the electrical conductivity, κ, as shown in Equation 3,

$$Z_{sol'n} = \frac{1}{\kappa}\left(\frac{\ell}{A}\right) \qquad [3]$$

where ℓ/A is the cell constant (ℓ is the current path length and A is the cross-sectional area). The cell constant (ℓ/A) is defined in Equation 4 for the coaxial cylindrical geometry as,

$$\frac{\ell}{A} = \frac{\ln\left(\frac{b}{a}\right)}{2\pi z} \qquad [4]$$

where z is the depth (or height) measurement, b is the inside diameter of the outer electrode, and a is the outside diameter of the inner electrode. Substituting Equation 4 into Equation 3 results in the relationship between the electrical conductivity (κ) and the impedance ($Z_{sol'n}$) of the solution in Equation 5.

$$\frac{1}{Z_{sol'n}} = \kappa \frac{2\pi z}{\ln\left(\frac{b}{a}\right)} \qquad [5]$$

Due to the differential manner of the high-accuracy technique, the electrical conductivity of the base slag is calculated from Equation 6,

$$\frac{d\left(\frac{1}{Z_{sol'n}}\right)}{dz} = \kappa \frac{2\pi}{\ln\left(\frac{b}{a}\right)} \qquad [6]$$

where $d(1/Z_{sol'n})$ is the change in inverse impedance of the solution for the particular depth increment (dz).

There are several advantages to the high-accuracy-height-differential technique that permits its applicability for measuring the electrical conductivity of the base slag.[5,7] Due to the concentricity and the rigid shape of the electrodes, the current travels through a well-defined

path. In addition, the cell constant is inversely proportional to the immersed depth of the coaxial cylindrical electrodes in the slag. (Equation 4) This is why there is no need for the high-accuracy-height-differential technique to be calibrated. Another advantage is that the measurements are possible at high temperatures because the (arbitrary) initial immersion of the electrodes does not require the exact surface to be known or visible. Therefore, the measurements can be made in a furnace at high temperatures where the base slag solution is obstructed from one's view.

As observed by Fried,[7] there are a couple of possible limitations to the high-accuracy-height-differential technique for measuring the electrical conductivity. The range of applicability with this technique on a laboratory scale is questioned for very high and very low conducting melts. The size and the depth increment of the laboratory scale electrodes are the two factors that limit the cell constant when measuring a wide range of electrical conductivities. In order to broaden the range of applicability (0.1-0.6 S/cm) from the original high-accuracy-height-differential technique developed by Schiefelbein,[5] the size of the depth increments was decreased by 400% and the inner electrode distance was increased by 71%. This allows a lower limit of impedance (higher electrical conductivity) to be measured by the high-accuracy-height-differential technique. Another limitation is the deviation from the assumption of equipotential electrodes. This deviation from equipotentiality would lead to the use of the transmission line model, thus eliminating the mathematical simplicity of the high-accuracy-height-differential technique.[5,7] The equipotentiality of the electrodes holds when the resistance of the electrodes is considerably less than the resistance of the melt. In this study, the conductivity of the graphite electrodes is considerably greater than that of the base slag (2-4 S/cm). These amendments to the

limitations permit the high-accuracy-height-differential technique for measuring electrical conductivity of the base slag.

III. EXPERIMENTAL

As previously stated, the volatilization rate was monitored for the base slag (60wt% CaF_2 – 20wt% CaO – 20wt% Al_2O_3). These experiments were conducted in a graphite crucible suspended in a purified argon atmosphere to prevent oxidation of the crucible material. The arrangement is schematically shown in Figure 3. The thermogravimetric (TG) balance that was utilized was a CAHN D-100 Series system with version 2.0 software.[8]

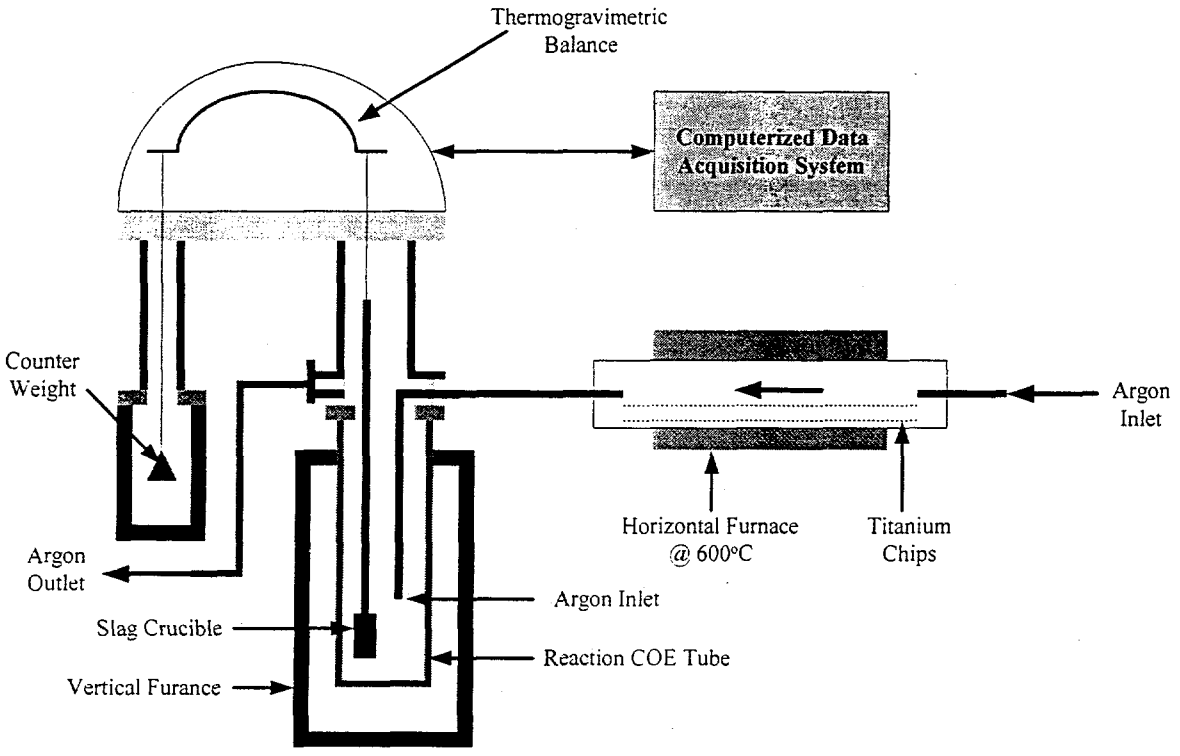

Figure 3: Thermogravimetry (TG) experimental setup

The experimental setup used to condense the volatile slag species onto a water-cooled copper coil is shown in Figure 4. Under an argon atmosphere, 250 grams of base slag was melted and held at 1500°C for six hours in a graphite crucible (6.985 cm I.D. x 128 cm deep). The condensed vapor was an amorphous powder. Therefore, an attempt was made to crystallize the

powder by annealing at 1000°C for analysis by X-ray diffraction. In order to determine the uncondensed volatile species, the volatile gas from the base slag was passed through a quadropole mass analyzer as shown in Figure 5.[9] The base slag (141.5 grams) was melted and held at 1500°C for six hours in a graphite tray (13.335 cm long x 3.81 cm wide x 25.4 cm deep). The volatile species were analyzed with the mass spectrometer while under a helium atmosphere.

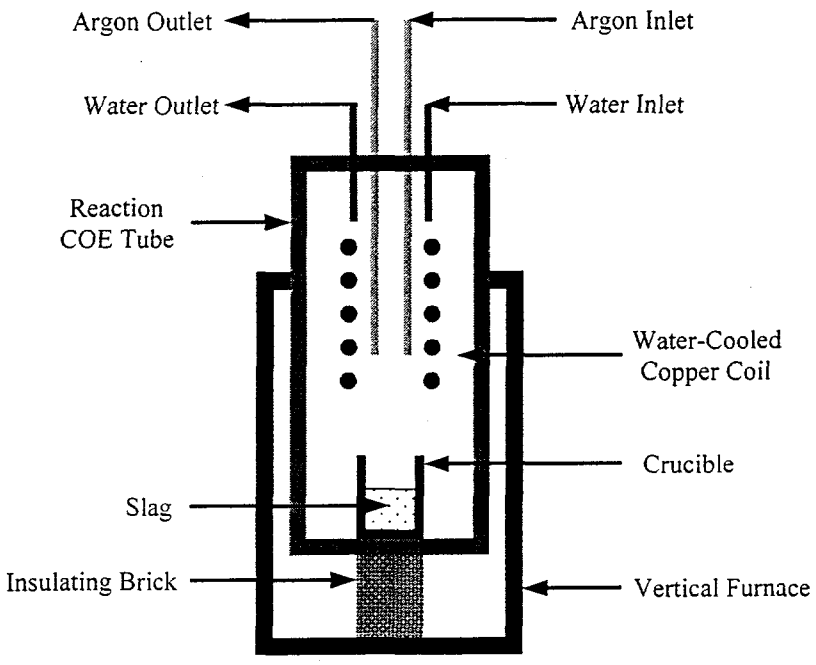

Figure 4: Experimental setup for condensation of volatile species

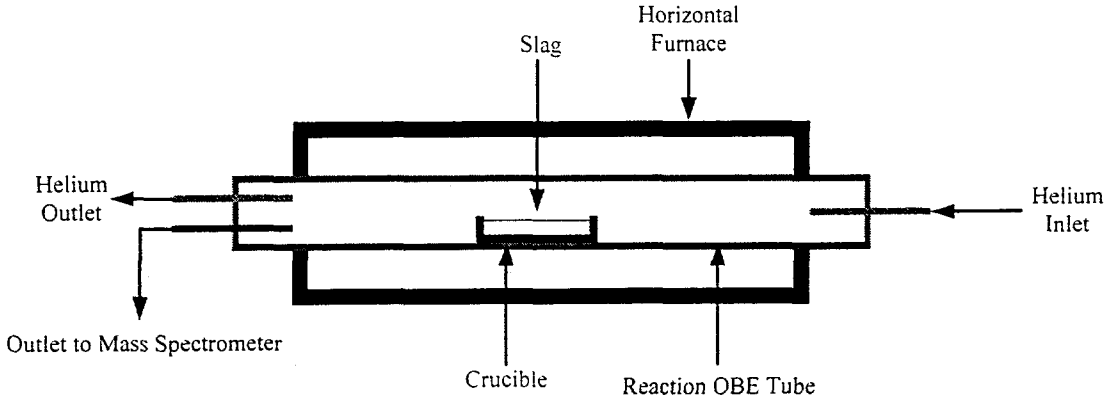

Figure 5: Experimental setup for mass analysis of uncondensed volatile species

Initially for the electrical conductivity study, each base slag component (CaF_2, CaO, and Al_2O_3) is dried separately in a furnace at approximately 150°C for 24 hours in order to remove any moisture. The dried slag components are mixed together according to the appropriate ratios (60wt% CaF_2 – 20wt% CaO – 20wt% Al_2O_3). The base slag is milled in a Teflon sealed bottle without any media for three hours in order to provide uniform mixture of the slag components. About one kilogram of base slag is hand packed in a graphite crucible (8.26 cm O.D. x 7.62 cm I.D.) for each experimental run. The graphite crucible with the base slag is lowered into a vertical tube furnace as shown in Figure 6.

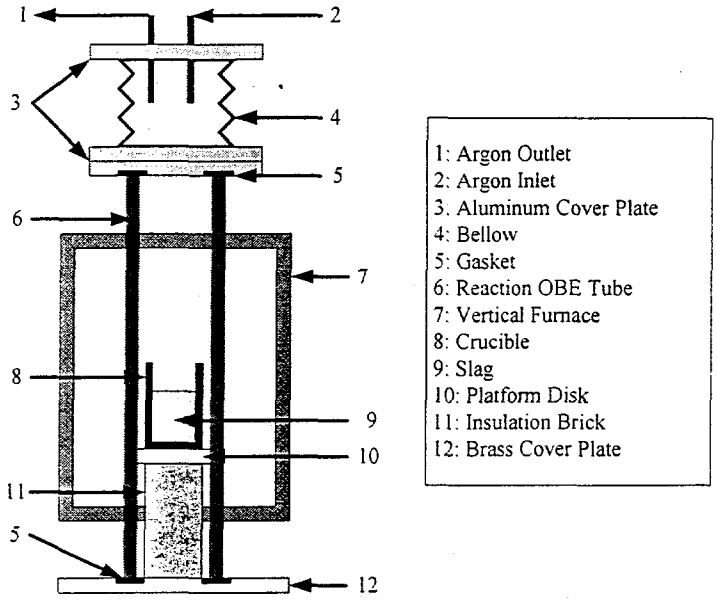

Figure 6: Furnace setup for high-accuracy-differential-height technique

The amount of base slag is approximately 8.26 cm high when melted. In order to eliminate the fringe effect from the measured impedance, the electrodes were lowered such that the lower fringe, or the current path, from the bottom of the electrodes is constant from one depth increment to the next. From Schiefelbein,[5] the recommended minimum spacing between the bottom of the coaxial cylindrical electrodes and the crucible floor (lower fringe immersion limit) is two times the interelctrode spacing ($2(b-a)$, where b is the inside diameter of the outer

electrode and *a* is the outside diameter of the inner electrode). For the experimental setup used in the present investigation for measuring the electrical conductivity of the base slag, the interelectrode spacing (*b*-*a*) between the inner and outer electrode is 2.54 cm.

If the distance between the bottom of the electrodes and the crucible floor is greater than the lower fringe immersion limit, as practiced in the present investigation, the lower fringe does not significantly contribute an error to the measurement method.[5] Otherwise, the lower fringe effect ($R_{sol'n}^{fringe}$) needs to be taken into consideration as shown in Equation 7.

$$\frac{d\left(\frac{1}{Z_{sol'n}}\right)}{dz} = \kappa \frac{2\pi}{\ln\left(\frac{b}{a}\right)} + \frac{d\left(\frac{1}{R_{sol'n}^{fringe}}\right)}{dz} \qquad [7]$$

If the crucible material is more conductive than the solution and the bottom of the electrodes comes within the lower fringe immersion limit, then there would be a convex deviation from linearity in the plot of inverse impedance ($1/Z_{sol'n}$) versus depth (z). Alternatively for a case where the crucible material was less conductive than the solution, one would expect concave deviation from linearity in the plot of inverse impedance ($1/Z_{sol'n}$) versus depth (z).

The electrochemical cell (Figure 7) consists of a graphite cylinder (3.18 cm I.D.) serving as the outer electrode and a graphite rod (6.35 mm O.D.) serving as the inner electrode. These concentric graphite electrodes are threaded into molybdenum rods (3.18 mm O.D.), thus providing the electrical contact to the leads of the impedance analyzer. The concentricity of the electrodes is maintained by a machined Boron Nitride separator that keeps the electrodes aligned. Alumina protection tubes electrically insulate the molybdenum electrodes passing through a series of cover plates and the bellow.

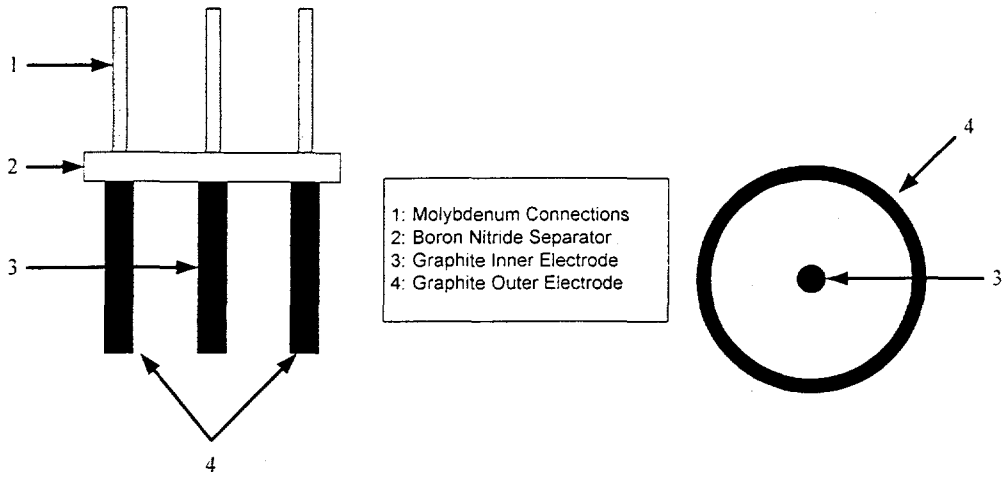

Figure 7: Electrochemical cell for high-accuracy-differential-height technique

Typically, electrical conductivity measurements of the base slag are made at three different temperatures in one experimental run. The measurements are performed in the order of the highest temperature to the lowest temperature. This method maximizes the range of the measured impedance since the resistance of the base slag decreases with increasing temperature as well as decreasing depth of the electrodes. Under an argon atmosphere, the base slag is melted and equilibrated for approximately two hours at the highest temperature. Microscopic evaluation of the quenched slag revealed that the slag was homogeneous. The surface of the base slag is determined by running AC impedance scans for successive depth increments of 2.54 mm (0.1"). The height of the electrodes is changed through the motion of a machined horizontal arm that is connected to a high precision linear rail. The motion arm is balanced by a counterweight system through a set of pulleys. A digital micrometer lowers onto the motion arm in order to adjust the depth of the electrodes. See Figure 8 for a schematic of the linear motion system. The surface of the slag is established as soon as the impedance drastically drops from one depth increment to the next. The zero reference or the top of the base slag is considered to be at this particular depth increment.

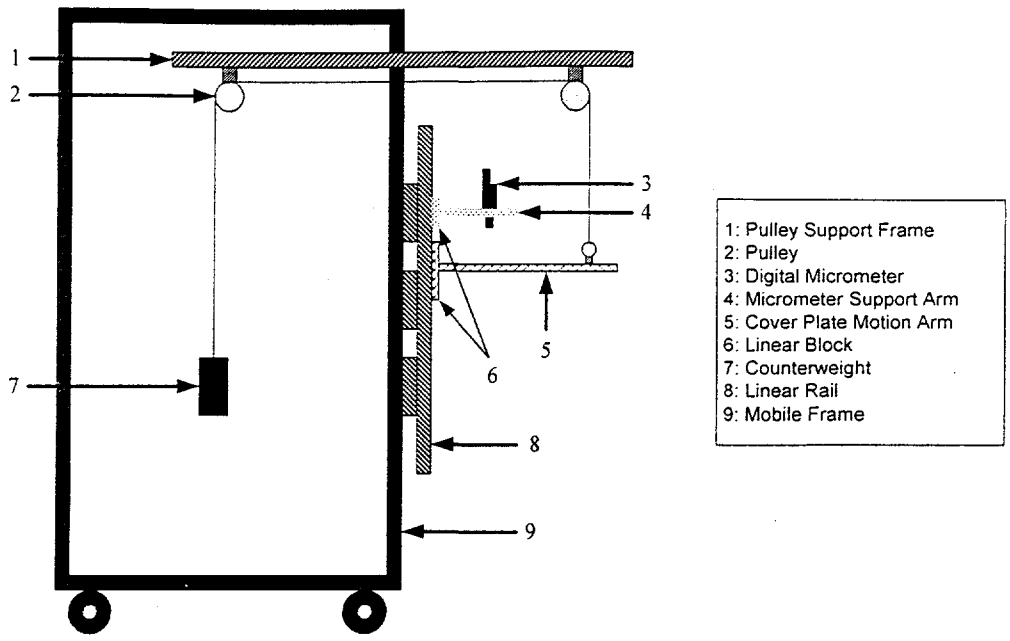

Figure 8: Linear motion setup for high-accuracy-differential-height technique

To prevent the surface fringe effects, the electrodes initially are lowered 1.02 cm (0.4") from the surface of the base slag. In order to measure the resistance of the base slag, a continuous AC impedance scan is run over a large frequency range (10^6 – 1 Hz) for a particular depth. The electrodes are lowered by increments of 0.254 mm by the digital micrometer and the AC impedance scans are repeated for each depth increment. These measurements are made for a total of 21 successive depth increments. This is sufficient statistically to determine the slope for the plot of inverse impedance ($1/Z_{sol'n}$) versus depth (z). Over this depth range, the temperature of the base slag changed by less than 2°C.

Next, the base slag is lowered to the second temperature in the same experimental run while the electrodes remain in the base slag at the final depth increment of the first temperature. The electrodes were not raised out of the base slag in between experimental temperatures, because the wetting behavior of the base slag with the electrodes created non-reproducible conductivity values. The contact angle of a previously wetted surface acts differently than that of a clean surface.[10] After 15 minutes of thermal equilibrium at the second temperature, the

electrodes were lowered further by 2.54 mm to serve as the starting point for the next set of AC impedance measurements at the second temperature. This additional 2.54 mm depth increment before starting the next set of measurements is rationalized by the change in density of the base slag as the temperature is decreased. With the lower temperature, there is an increase in the density of the base slag, and the height of the base slag decreases. The additional 2.54 mm depth increment ensures that the position of the electrodes at the slag-electrode interface is clean and has not been previously wetted by the slag. After the second experiment is completed, the furnace is ramped down to the third and final temperature and this AC impedance measurement procedure is repeated. After the final measurement at the third temperature, the electrodes are raised out of the base slag and the furnace is cooled down to room temperature.

The baseline electrical conductivity measurement of the base slag for comparison with the high-accuracy-height-differential technique was performed using an AC impedance method with two point electrodes as shown in Figure 9. The cell constant for these baseline experiments was determined by measuring the electrical conductivity of a 0.01N KCl standard solution at 25°C. The base slag was heated in an alumina crucible under a purified argon atmosphere.

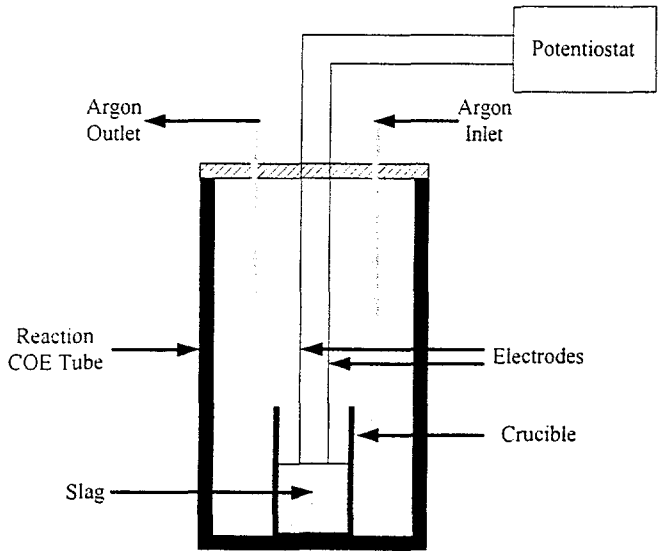

Figure 9: Experimental setup for two point electrodes technique

IV. RESULTS

The typical result of the thermogravimetric (TG) analysis on the base slag is shown in Figure 10. For each volatilization experiment, there was initially some weight loss, above 300°C (Figure 10), that was attributed to the evaporated moisture originally present in the base slag powder. The calculated evaporation rates of the base slag as a function of temperature are listed in Table I. These rates were plotted as a function of temperature in Figure 11 and followed an Arrhenius behavior. The volatilization rate, R in g/cm^2-sec, of pure base slag is expressed as a function of temperature, T in Kelvin, in Equation 8.

$$R = 3445.26 \exp\left(-\frac{37955.09}{T}\right) \qquad [8]$$

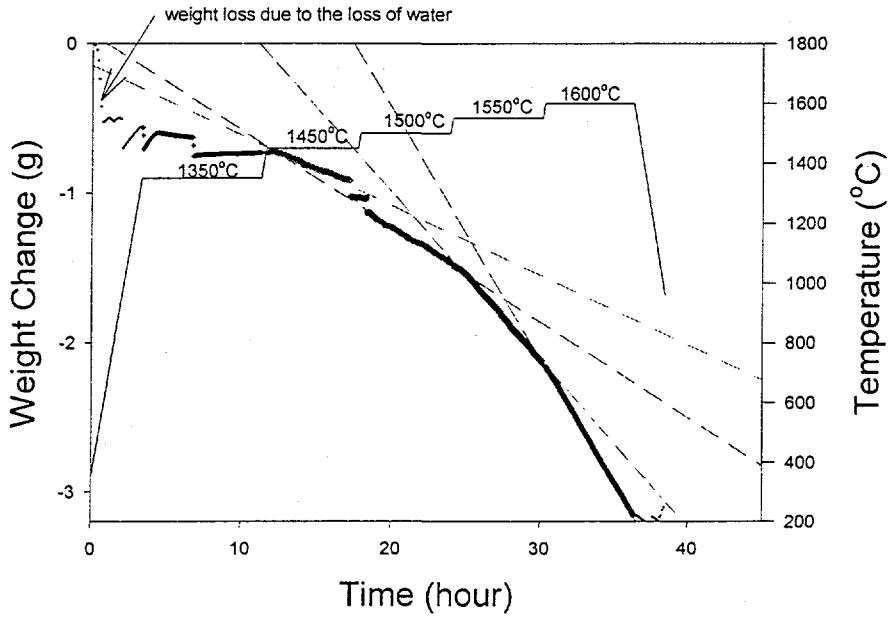

Figure 10: Thermogravimetric experiment with base slag

Table I: Volatilization rates of base slag with varying amounts of ceria

Experiment Type	Base Slag Mass (g)	Temperature (^{o}C)	Volatilization Rate (g/cm^2-sec)
Pure Base Slag	37.687	1450	1.010E-06
Pure Base Slag	37.687	1500	1.500E-06
Pure Base Slag	37.687	1550	3.280E-06
Pure Base Slag	37.687	1600	5.560E-06

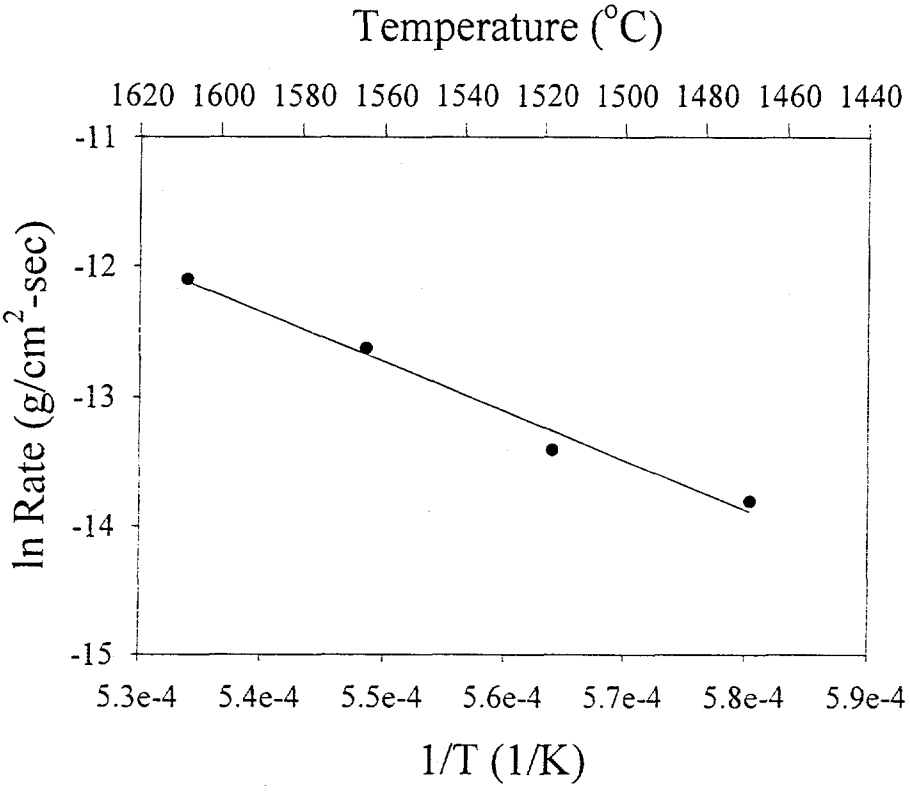

Figure 11: Arrhenius plot of base slag volatilization rates

From the condensed vapor collected, the X-ray diffraction pattern showed a presence of CaF_2. (Figure 12) The analysis by the mass spectrometer revealed AlF_3 among the uncondensed volatile species. (Figure 13) The low volatilization rates, which were measured in this study, indicate that the base slag will remain relatively homogeneous and unchanged in composition during the electrical conductivity experiments; each experimental set (three temperatures) is

completed within six hours and approximately one gram of base slag is lost from a total of 1000 grams.

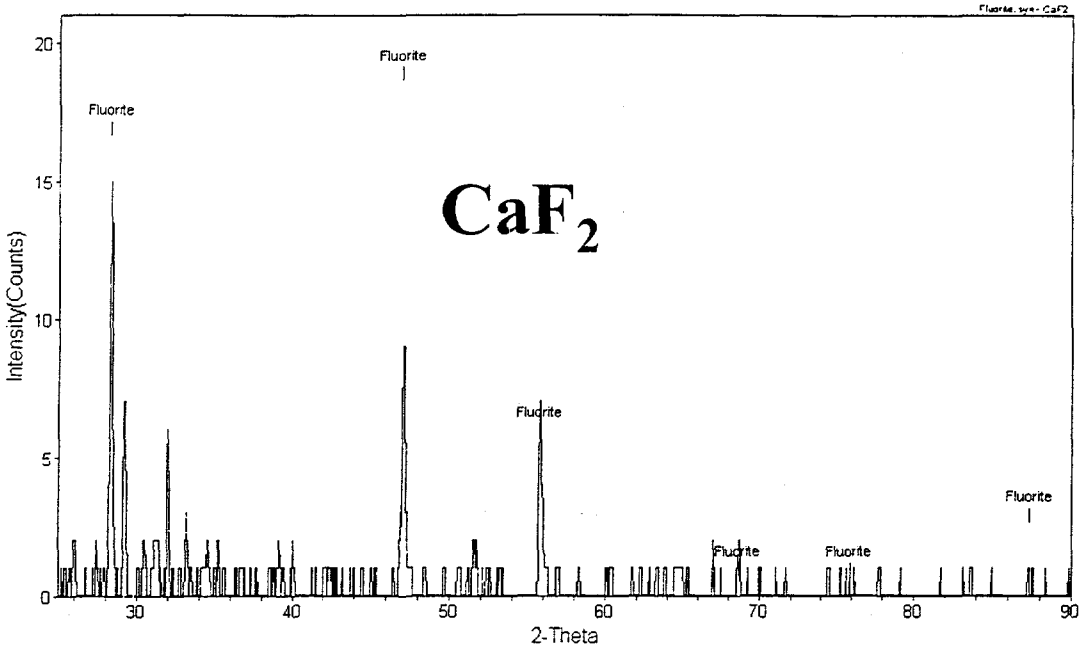

Figure 12: X-ray diffraction pattern of CaF_2 peaks

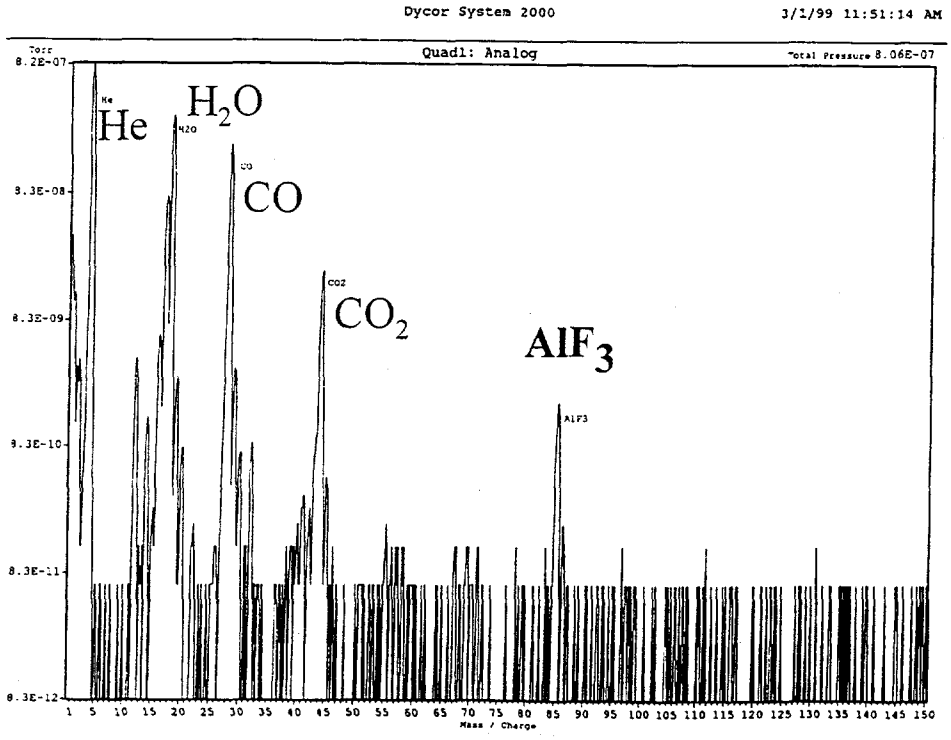

Figure 13: Mass spectroscopy analysis

The accuracy of the height-differential technique was checked using two different compositions (0.1 S/cm and 0.01 S/cm) of the NIST standard KCl solution. The conductivity values obtained were within 5%. The minimum initial depth of the electrodes required to eliminate surface fringe effects was experimentally determined to be 1.02 cm below the established surface of the solution. The resolution of the digital micrometer for accurately measuring the impedance signal as a function of the depth increments was determined to be 0.254 mm (0.01"). The accuracy of the micrometer for 0.254 mm depth increments, as measured from the micrometer readings, was certified within ±10% of the actual depth increments by utilizing a blank experimental run at room temperature. See Table II. Larger deviations between the actual depth increment and the micrometer reading occurred with smaller depth intervals of 0.127 mm (0.005"). See Table III. From these results, it is clear that the actual depth of the electrodes is much closer to the digital micrometer reading for the 0.254 mm depth increments rather than the 0.127 mm depth increments.

Table II: Accuracy results of 0.254 mm depth increments

Micrometer Depth Readng (mm)	**Actual Depth (mm)**	**Actual Depth Increment (mm)**	**% Error**
0.000	0.000	-	-
0.254	0.254	0.254	0.0%
0.508	0.533	0.279	10.0%
0.762	0.787	0.254	0.0%
1.016	1.041	0.254	0.0%
1.270	1.346	0.305	20.0%
1.524	1.549	0.203	20.0%
1.778	1.829	0.279	10.0%
2.032	2.083	0.254	0.0%
2.286	2.311	0.229	10.0%
2.540	2.565	0.254	0.0%
2.794	2.845	0.279	10.0%
3.048	3.124	0.279	10.0%
3.302	3.353	0.229	10.0%
3.556	3.581	0.229	10.0%

Table III: Accuracy results of 0.127 mm depth increments

Micrometer Depth Readng (mm)	Actual Depth (mm)	Actual Depth Increment (mm)	% Error
0.000	0.000	-	-
0.127	0.076	0.076	40.0%
0.254	0.254	0.178	40.0%
0.381	0.356	0.102	20.0%
0.508	0.508	0.152	20.0%
0.635	0.635	0.127	0.0%
0.762	0.762	0.127	0.0%
0.889	0.965	0.203	60.0%
1.016	0.965	0.000	100.0%
1.143	1.118	0.152	20.0%
1.270	1.219	0.102	20.0%
1.397	1.346	0.127	0.0%
1.524	1.575	0.229	80.0%
1.651	1.626	0.051	60.0%
1.778	1.727	0.102	20.0%
1.905	1.880	0.152	20.0%
2.032	2.057	0.178	40.0%
2.159	2.083	0.025	80.0%
2.286	2.692	0.610	380.0%
2.413	2.616	-0.076	40.0%
2.540	2.743	0.127	0.0%

A typical experimental run of the base slag, which consists of three temperatures (1550°C, 1500°C, and 1460°C), results in a plot of the inverse impedance of the solution versus the particular depth increment for each temperature. (Figures 14-16) The slope from this linear plot is used to calculate the electrical conductivity (κ) of the base slag at the specific temperature. (Equation 6) The electrical conductivity measurements from the high-accuracy-height-differential technique showed a single Arrhenius behavior for the base slag. See Figure 17. The measured values of the electrical conductivity are listed in Table IV. From these measured values, the linear regression produced an Arrhenius equation shown in Equation 9,

$$\ln\kappa = 6.593 - \frac{10175}{T} \qquad [9]$$

where κ is the electrical conductivity in S/cm and T is the temperature in Kelvin. The Arrhenius behavior indicates that the conduction mechanism remains primarily unchanged; the conduction mechanism is most likely dominated by the F ions.

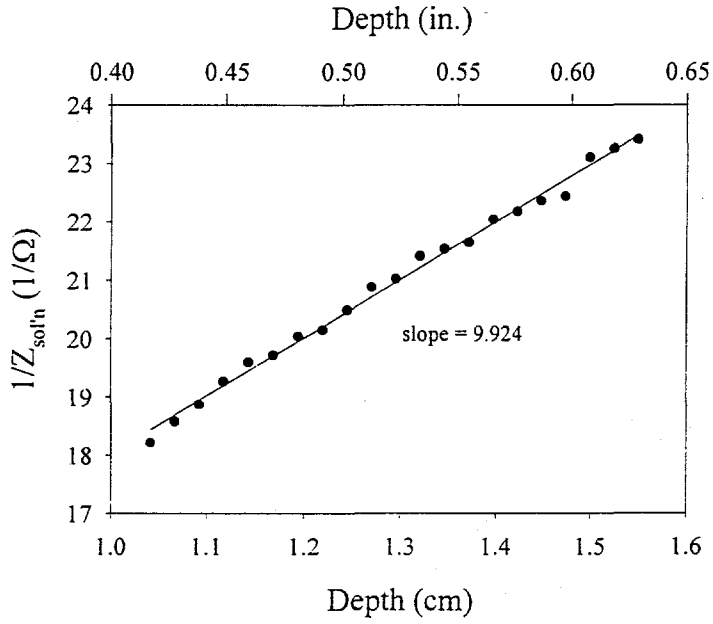

Figure 14: Plot of inverse impedance versus depth at 1550°C

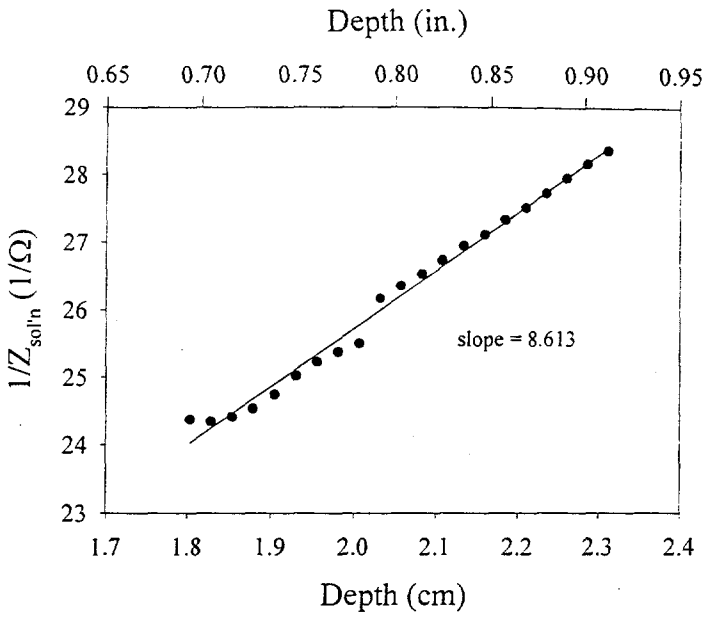

Figure 15: Plot of inverse impedance versus depth at 1500°C

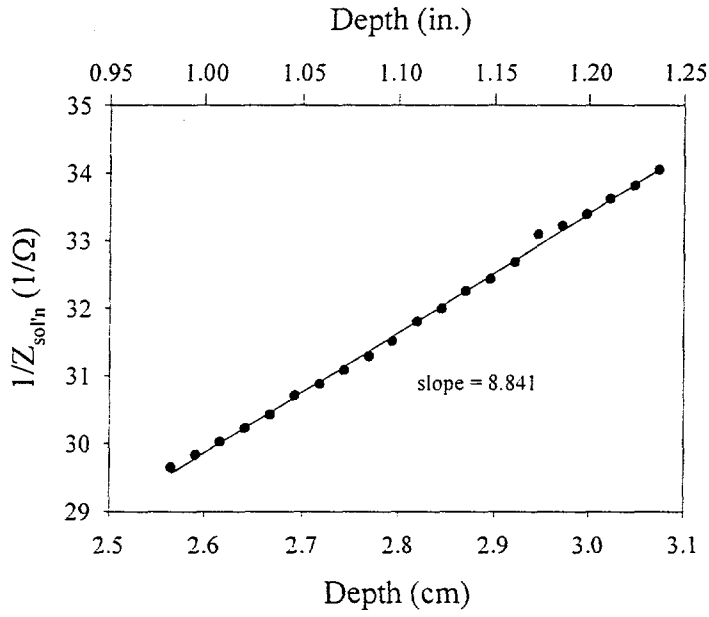

Figure 16: Plot of inverse impedance versus depth at 1460°C

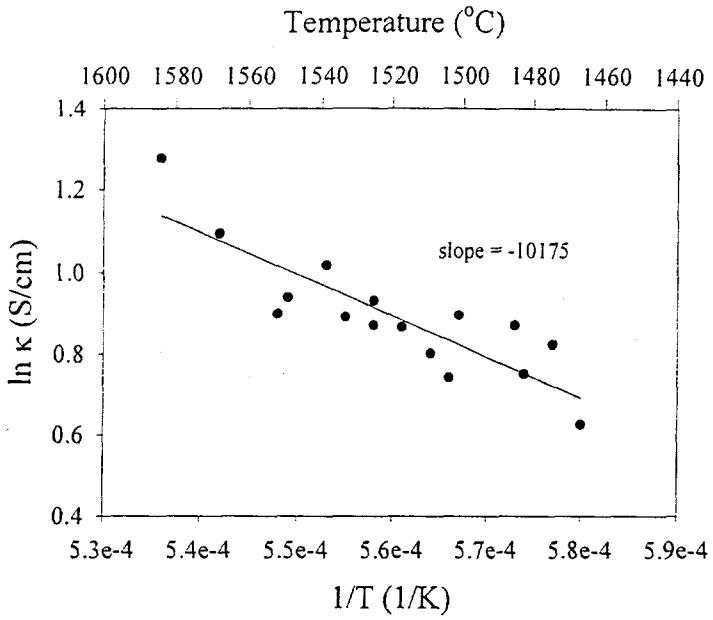

Figure 17: Arrhenius plot of base slag

Table IV: Electrical conductivity values measured

Conductivity (S/cm)	**Temperature (°C)**
3.59	1592
2.99	1571
2.46	1553
2.56	1550
2.77	1536
2.44	1528
2.39	1520
2.54	1520
2.38	1511
2.23	1500
2.10	1493
2.45	1490
2.39	1471
2.12	1470
2.28	1460
1.87	1450

At 1600°C, the electrical conductivity is extrapolated to a value of 3.19 S/cm using Equation 9. This value closely agrees to several reported values in literature. For instance, it is within 0.2% of the Slag Atlas[11], 0.4% of Mills and Keene[3], 8.8% of Hara, et al.[12], and finally within 11.1% of the baseline measurement made with the two point electrodes. The comparison

of the Arrhenius behaviors for the high-accuracy-height-differential technique, the Slag Atlas[11], and the baseline measurement is plotted in Figure 18. This plot shows nearly identical trends for the high-accuracy-differential-height technique and the Slag Atlas[11] while the baseline measurement appears to be lower and parallel to the high-accuracy-height-differential technique. Since the baseline measurement utilized a two point electrodes method, the measured cell constant could have been inaccurate. For the two point method, the current paths in the base slag and the standard KCl solution are not identical because their conductivities and measurement temperatures are different. Therefore, the cell constant measured with a KCl solution at room temperature will be different from the actual cell constant when using the base slag. With only the cell constant being different, one would expect to observe an Arrhenius behavior that is parallel to the high-accuracy-height-differential technique as seen in Figure 18. Hara, et al.[12] measured the electrical conductivity using four point electrodes where the cell constant was calibrated with CaF_2 at 1600°C. Thus, these measurements are more reliable than those made with the two point electrodes because they were calibrated at high temperature with a similarly conductive material. Yet, the current path of the four point electrodes technique is not as well confined or defined as the presently investigated coaxial system of electrodes. Hence, errors in the cell constant measurements can get magnified. Like most traditional methods, the four point electrodes technique also does not take into account the upper and lower fringe effects as the high-accuracy-height-differential technique. The very similar behavior between the high-accuracy-height-differential technique and the Slag Atlas[11], as seen in Figure 18, is reasonable since each method employs a similar cell geometry. As previously stated, the high-accuracy-height-differential technique utilized coaxial cylindrical electrodes while the Slag Atlas[11] used a similar Platinum ring and rod technique. Even though these techniques both have well defined

current paths, the high-accuracy-height-differential technique is calibration free and therefore quicker and easier to conduct. Thus with the high-accuracy-height-differential technique, there is no need to obtain a solution for measuring the cell constant that is relatively similar to the conductivity of the unknown solution (base slag). This also takes out the guess work and the associated uncertainty from the measurement.

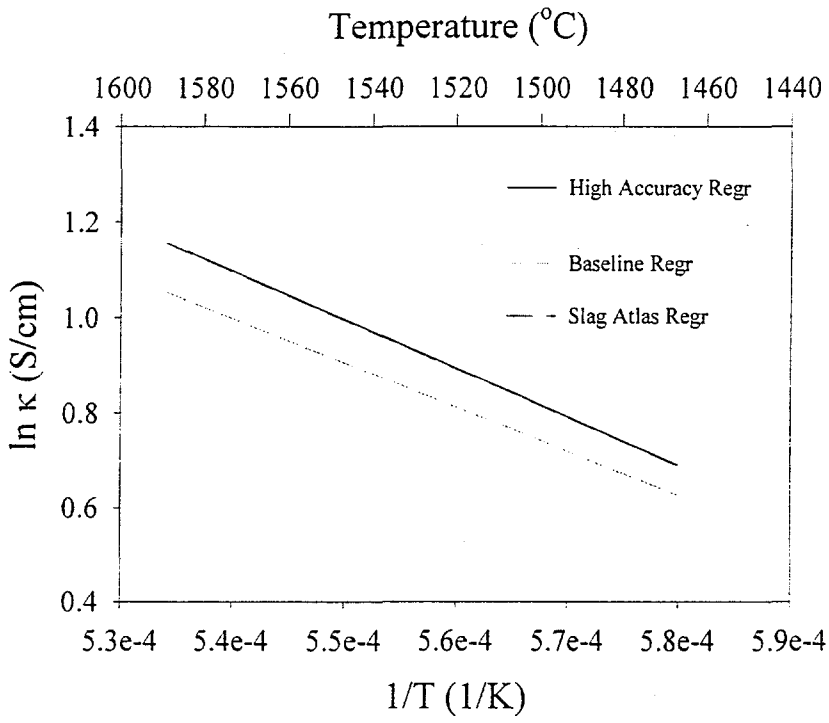

Figure 18: Arrhenius plot comparison of different techniques

Future experiments include measuring the electrical conductivity of the base slag with separate additions of the surrogate oxide (CeO_2) for the radioactive contaminants (uranium and plutonium) and the surface enhancer (TiO_2). It is anticipated that the semiconducting nature of ceria (CeO_2) and titania (TiO_2) could effectively alter the electrical conductivity of the base slag.

V. CONCLUSION

The volatilization study revealed a low volatilization rate of the base slag. The volatilization rates for the base slag displayed an Arrhenius behavior. The volatile species of the base slag were also determined to be mainly CaF_2 and AlF_3. The volatilization study confirmed that the base slag composition does not essentially change during the electrical conductivity experiments. The improved high-accuracy-height-differential technique provided an effective method for measuring the electrical conductivity of highly conductive melts, such as the ESR slag, because of the increased electrochemical cell geometry and the capability to make smaller high precision depth increments. The height-differential part of this technique permits the measurements to be made without prior calibration of the cell constant on a similarly conductive solution at high temperatures. Thus, the high-accuracy-height-differential technique eliminates the critical and time consuming step of measuring the cell constant that is present in the traditional electrical conductivity measurement methods. The electrical conductivity of the base slag was measured and followed an Arrhenius behavior. The measured values of the electrical conductivity were compared with those found in literature. The electrical conductivity of the base slag is such that it provides a reasonable melt rate along with sufficient Joule heating for the Electroslag Remelting (ESR) process. Future experiments are planned to monitor the effects of the individual additions of the surrogate oxide (CeO_2) for the radioactive contaminants (uranium and plutonium) and the surface enhancer (TiO_2) on the electrical conductivity and the volatilization behavior of the base slag.

VI. ACKNOWLEDGEMENTS

This research is sponsored by the U.S. Department of Energy through Sandia National Laboratory, Albuquerque, NM. The authors gratefully acknowledge the following people from the Materials Group at the Department of Manufacturing Engineering at Boston University: William Chernicoff, Edward Y. Chiang, Dr. Kuo Chih Chou, Charles D'Angelo, Timothy Keenan, Helmut Lingertat, Scott A. MacDonald, Robert Sjostrom, Sesha Varadarajan, and Dr. David Woolley.

VII. REFERENCE

1. T.E. Bechtold: "Winco Metal Recycle Annual Report FY 1993", WINCO-1172, Prepared for the U.S. Department of Energy, Idaho Field Office, 1993.

2. J.M. R. Buckentin: Ph.D. Thesis, Oregon Graduate Institute of Science & Technology, Oregon, 1996.

3. K.C. Mills and B.J. Keene: International Metals Reviews, 1981, No. 1, pp. 21-69.

4. M. Choudhary and J. Szekeley: Metallurgical and Materials Transactions B, June 1981, vol. 12B, pp.418-421.

5. S.L. Schiefelbein: Ph.D. Thesis, Massachusetts Institute of Technology, Cambridge, MA, 1996.

6. A.J. Bard and L.R. Faulkner: Electrochemical Methods, John Wiley & Sons, Inc., New York, NY, 1980, pp. 322-324.

7. N.A. Fried: Ph.D. Thesis, Massachusetts Institute of Technology, Cambridge, MA, 1996.

8. A. Agarwal: M.S. Thesis, Massachusetts Institute of Technology, Cambridge, MA, 1998.

9. W. P. Chernicoff, C. J. MacDonald, H. Gao, D. Woolley, K. C. Chou, and U.B. Pal: Global Symposium on Recycling, Waste Treatment and Clean Technology, San Sebastian, Spain, September 1999.

10. S.L. Schiefelbein and D.R. Sadoway: Metallurgical and Materials Transactions B, December 1997, vol. 28B, pp. 1141-1149.

11. V.D. Eisenhüttenleute: Slag Atlas, Verlag Stahleisen m.b.H., Düsseldorf, Germany, 1981, pp. 258-282.

12. S. Hara, H. Hashimoto, and K. Ogino: Transactions of the Iron and Steel Institute of Japan, 1983, vol. 23, no. 12, pp. 1053-1058.